Supplementary Information for

Enhancing Binding Affinity Predictions through Efficient Sampling with re-engineered BAR Method: Test on GPCR Targets

Minkyu Kim, Jian Jeong, Donghwan Kim, Sangbae Lee*, and Art E. Cho*

This document contains:

Supplementary Information (SI) Theory

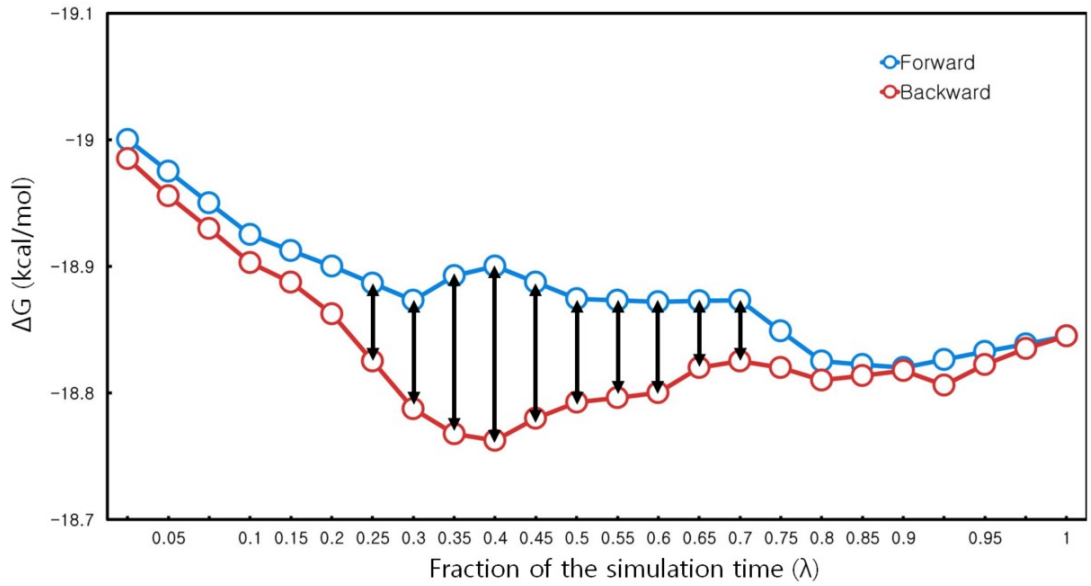

SI Figure S1. (Related to main Theory & Method section). Free energy convergence with time. Computed free energy differences are shown as a function of time to access equilibration and convergence. Here, we show free energy estimates resulting both from forward (light blue) time series, and what we would obtain if the data were analyzed in a time-reverse manner (red) using the same amount of data, as discussed in the Method text. As shown in X-axis, 24 scaling factors (λ) using inequivalent manner (from 0 to 0.1 and from 0.9 to 1) for smooth passing its energy barrier.

Supplementary Information (SI) Methods

Analyses for MD simulation and binding free energy

Calculating the ligand binding free energy using the alchemical free energy method – BAR (Bennett acceptance ratio)

: We have calculated the binding free energy (ΔG) of ligand and GPCR receptor using the Bennett Acceptance Ratio (BAR) algorithm in the GROMACS package. BAR method combines the information normally used for forward and reverse free energy perturbations. This can be expressed as function of a coupling parameter, λ, which indicates the level of change that has taken place between two states (ligand-bound and unbound), the extent to which the Hamiltonian has been perturbed and the system has been transformed. Simulations conducted at different values of λ allow us to plot a $\partial H/\partial \lambda$ curve, from which ΔG is derived. Transformations from ligand-bound (λ = 0) to ligand-free (λ =1) in our study were performed in non-equidistant λ spacing from 0 to 1 for decoupling Coulombic and van der Waals interaction using 0.8 ns of simulation for each window (SI Figure S1).

Key Computational Steps and Parameters

: Binding-free-energy calculations performed with molecular-dynamics (MD) simulations may appear algorithm-agnostic, yet their outcomes still depend sensitively on user-specific protocols. The most critical factor for best results lies in how accurately the setup and equilibration of the protein–ligand complex are designed to reflect the experiments.

Accordingly, we adopted the multi-step equilibration scheme summarized in SI Table S1 to ensure that the solute accurately mirrors experimental conditions. This careful preparation was essential to ensure the reliability of the subsequent MD-based binding free energy calculations.

SI Table S1. Multi-Step Preparation Workflow for MD BFEs

Steps	Explanation	Restraints	
		Position (kcal/mol)	Distance (kcal/mol)
Step1	Energy minimization	X	X
Step2	Equilibration (NVT)	5	5
Step3	Equilibration (NVT)	4	5
Step4	Equilibration (NpT)	3	5
Step5	Equilibration (NpT)	2	5
Step6	Equilibration (NpT)	1	5
Step7	Equilibration (NpT)	X	5
Step8	Equilibration (NpT)	X	X
Step9	Production (NpT)	X	X

*X = 0 kcal/mol

Another strength of the BAR method lies in its adaptability through the use of unevenly distributed scaling factors (λ), unlike other binding free energy methods that rely on fixed or uniformly spaced λ intervals. Instead of employing a uniform λ schedule from 0 to 1, we adopted a non-uniformly distributed λ scheme, placing denser sampling near the endpoints ($\lambda \approx 0$ and $\lambda \approx 1$). This design ensures sufficient sampling in regions of rapid energy change during the early and late stages of ligand decoupling, where the soft-core potential function exhibits its highest sensitivity. This type of adaptive λ distribution enhances both the numerical stability and accuracy of BAR-based free energy calculations, making it especially well-suited for structurally flexible systems like GPCRs, where careful management of state overlap is crucial.

Superiority of our MIND-BAR over FEP

: Unlike FEP, the BAR method utilizes both forward and backward perturbation data, which is central to its statistical robustness. Importantly, the scaling factor (λ) used in BAR does not require equal spacing, allowing it to be redistributed based on state overlap, which is particularly advantageous for complex systems like GPCRs. In GPCR–ligand systems, the high flexibility of the binding pocket necessitates careful sampling, making equilibration and production runs critical prior to accurate binding free energy calculation. For this reason, we applied both position and distance restraints during the equilibration phase to minimize ligand displacement. We then performed five independent production runs using different random seeds and selected the most structurally stable ensemble as the starting point for free energy computation. This protocol produced less variation in output compared to other methods.

SI Table S2. Comparative Summary of GPCR BFE Protocols

Journal	Chem.Sci.	ACS Omega, 2016	J. Chem. Inf. Model. 2020	Angew. Chem. Int. Ed. 2023
Corresponding Authors	A Cho. S Lee.	AP IJzerman T Beuming	Cde Graaf G Tresadern	P Gmeiner J Carlsson
Affiliation	inCerebro Atomatrix	Leiden Univ. Schrodinger	Sosei Heptares Janssen Pharma.	Uppsala Univ. FAU
Method	MIND-BAR	FEP+	FEP+, MMGBSA	FEP+
Target	β_2AR A_{2A}R	A_{2A}R, dOR CXCR4, β_1AR	A_{2A}R OX2	β_2AR
Equilibration	EM: NVT EQ:PR+DR	EM: NVT EQ: NPT with PR	EM: NVT EQ: NPT with PR	EM: NVT EQ: NPT with PR
Production	50ns x 5 runs	No	No	No

*EM: Energy Minimization, EQ: Equilibration. PR: Position restraints. DR: distance restraints.

Comparison Between MIND-BAR and Other Binding Free Energy Methods, and Its Suitability for GPCRs

: A variety of alchemical binding free energy methods have been applied to transmembrane proteins, particularly GPCRs, which are among the most structurally complex and pharmacologically important membrane targets. In this study, we compared the BAR (Bennett Acceptance Ratio) algorithm—used as the core method—with several other representative approaches, highlighting its distinct advantages for GPCR systems.

(1) Use of Both Forward and Backward Data for Enhanced Statistical Accuracy: GPCRs are flexible, dynamic membrane proteins where ligand binding often induces transitions across multiple conformational states. The MIND-BAR method estimates free energy differences by utilizing both forward (A→B) and backward (B→A) perturbation data, resulting in reduced standard error and greater resistance to sampling noise compared to FEP. Therefore, BAR is particularly well-suited for GPCR systems where sufficient state overlap is attainable. (Bennett, C. H. (1976). J. Comput. Phys., 22, 245–268.)

(2) Superior Sampling Efficiency and Convergence: Due to the narrow and flexible nature of GPCR binding pockets, convergence in free energy calculations is often hindered by sampling bias. The MIND-BAR method used in this study integrates data across multiple λ states, improving convergence and minimizing free energy gradient errors, especially at the extreme λ ends. This approach demonstrated greater robustness compared to TI-based methods.

(3) Flexibility and Broad Applicability Across Platforms: MIND-BAR is compatible with various molecular dynamics packages, including GROMACS, AMBER, and CHARMM, and can be applied via built-in or external postprocessing tools. It is particularly effective for GPCR–ligand complexes with well-defined topologies and is fully compatible with dual topology schemes (Lee et al., J. Phys. Chem. B, 2014). In contrast, TI requires precise force integration and gradient smoothness, which can be more demanding in flexible membrane protein systems.

(4) Validated in Real GPCR Applications: MIND-BAR free energy calculations have shown excellent agreement with experimental binding affinities, typically within an RMSE of ~1.0 kcal/mol. The method has been successfully applied to a range of GPCR targets, including A_{2A}AR, β_2AR, OX2R, and CXCR4, demonstrating its robustness and growing adoption in structure-based drug design workflows.

SI Table S3. Key Strengths of MIND-BAR in GPCR Binding Free-Energy Studies

Aspect	Advantage of MIND-BAR	Comparison with Others.
Statistical Accuracy	Utilizes both forward and backward data; minimum variance estimator	FEP is uni-directional and prone to bias
Sampling Convergence	Integrates across λ states; improves slow convergence	TI is sensitive to gradient smoothness
Computational Efficiency	High accuracy relative to cost; easy post-processing automation	LIE is simple, but less accruable
Structural Suitability for GPCRs	Handles flexible binding pockets effectively	TI requires smooth potential transitions
Validation in GPCR systems	Widely applied to real GPCR targets; robust performance shown	BAR is increasingly used as a standard algorithm

Representative structure from RMSD-based clustering

: The structures shown in figures of main article are representative structures from the highest population conformation cluster for each ligand-GPCR complex. We first clustered the conformations in the MD trajectories by their root mean square deviation (RMSD) of the C_α atoms in the transmembrane helices, using the *gmx cluster* module in GROMACS with *gromos* clustering algorithm. An RMSD cut-off of 2.0Å was used on the MD trajectories containing snapshots taken every 20 ps. The representative structure was calculated as the frame that has the lowest RMSD compared to the average structure of the most populated conformational cluster.

Calculation of RMSD and RMSF

: To compare the relative difference between trajectories and to determine whether each simulation had converged and fluctuated, the Cα-RMSD (root means square deviation) and the RMSF (root means square fluctuation) of GPCR were calculated using the *g_rms* and *g_rmsf* modules of GROMACS. The average structure calculated from the combined trajectories (3 trajectories) of the last 30ns for each system was used as the reference structure for the RMSF calculations.

Calculation of SDF (Spatial distribution function)

: The spatial distribution function used for selective agonist movements in the binding site of β_1AR (SI Figure S2) was calculated using program tool '*gmx spatial*' in the GROMACS package, and visualized using PyMOL. This represents the density of nitrogen and oxygen atoms (indicated with the blue and red dots, respectively) within the each ligand over all the MD snapshots.

Polar and non-polar ligand-GPCR interaction

: The polar and non-polar interaction energy components shown in the main Figure 2 were calculated using GROMACS. Non-bond interaction energy included the Columbic and Lennard-Jones potentials (as the terms of polar and non-polar interactions) for β_1AR receptor for each protein-ligand interaction energy. For this, first, we identified all systems that make contacts in more than 40% from the last 30 ns of MD simulation snapshots. The polar interactions (hydrogen bond interactions) were calculated between hetero-atoms (N, O) with a distance cutoff of 3.5 Å and angle cutoff of 120° using our in-house tool. The van der Waals (vdW, non-polar) contacts were calculated with a distance cutoff of 4.0 Å between two sidechain carbon atoms using VMD tool '*contactFreq.tcl'*.

Volume of the ligand binding site

: We have calculated the volume of the ligand binding site in two different conformational states of β_1AR (for main Figure 2) and A_1AR/A_3AR (for main Figure 4) across all the MD trajectories. We first defined a 12×12×12 Å^3 box centered at the centroid position of the ligand structure after equilibration. After filling the defined box with grid points at 1 Å resolution, we systematically deleted the grid points that overlapped with any atom, based on the van der Waals clashes. A spherical region positioned at the box center with 4 Å radius was defined as the core region. These steps were carried out automatically by program POVME.

MIND mutation for *in-silico* Mutagenesis

: To introduce specific mutations from wild-type protein residues, we employed our in-house **MIND-mutation** tool. This proprietary method is designed to be optimized for the CHARMM force field used in this study and supports all 20 standard amino acids. For each desired single-point mutation, multiple rotamers were generated from the wild-type residue, and the most stable conformer was selected based on calculated interactions with surrounding protein residues and/or ligand atoms within a 5 Å radius.

SI Table S4. Overview of datasets used in case individual study.

Cases	Target	PDB	State	Resolution (Å)	Ligand	RSCC	RSR
Case1	β_1AR	2Y03	Inactive	2.85	Isoprenaline	0.97	0.21
		6H7J	Active	2.80	Isoprenaline	0.92	0.21
		2Y04	Inactive	3.05	Salbutamol	0.97	0.28
		6H7M	Active	2.76	Salbutamol	0.93	0.22
		2Y01	Inactive	2.60	Dobutamine	0.96	0.19
		6H7L	Active	2.70	Dobutamine	0.92	0.20
		4BVN	Inactive	2.10	Cyanopindolol	0.96	0.11
		6H7O	Active	2.80	Cyanopindolol	0.98	0.16
Case2	A_1AR	5N2S	Inactive	3.30	PSB36	0.92	0.27
	A_{2A}AR	5N2R	Inactive	2.80	PSB36	0.94	0.24
Case3	A_1AR	5UEN	Inactive	3.20	DU172	0.83	0.37
	A_3AR	-	Inactive	-	Homology[a]		
Case4	A_{2A}AR	3EML	Inactive (wild)	2.60	ZM241385	0.94	0.17
		3PWH	Inactive (MUT)	3.30	ZM241385	0.85	0.39

[a]A_3AR (old pdb code of 1OEA) was homologically modeled using the available AlphaFold2 predicted structure from the Uniprot website, as it has been removed from the PDB entry.

Supplementary Information (SI) Results

SI Table S5. (Related to main Figure 1)

β_1AR	exp (pK_D)	ΔG (kcal/mol)	PDB code
ISO-L	8.16	-12.35	2Y03
ISO-H	8.62	-16.13	6H7J
SAL-L	5.92	-11.05	2Y04
SAL-H	7.8	-13.5	6H7M
DOB-L	6.86	-12.98	2Y01
DOB-H	8.97	-15.83	6H7L
CYP-L	9.99	-16.21	4BVN
CYP-H	9.85	-15.99	6H7O

SI Table S6. (Related to main Figure 2) Percentage analysis of polar and non-polar interactions between respective agonist and the active or inactive state of β_1AR, based on the entire MD trajectories. Polar interactions are shown in red, while non-polar interactions are in blue.

Isoprenaline			Dobutamine			Salbutamol			Cyano-pindolol		
	AC[a]	IN[b]		AC	IN		AC	IN		AC	IN
F201	59%	53%	F201	96%	41%	F201	62%	85%	F201	72%	54%
D121	79%	72%	D121	100%	74%	D121	88%	100%	F325	58%	-
F306	49%	59%	V122	54%	58%	N329	54%	59%	D121	100%	92%
N329	58%	54%	F307	77%	62%	V125	61%	-	F306	77%	48%
V125	54%	-	S211	98%	-	V122	57%	66%	Y333	-	74%
V122	54%	55%	S212	-	48%	F307	62%	41%	V125	62%	51%
S211	-	77%	W330	93%	45%	S215	90%	93%	V122	75%	63%
S215	-	93%	G98	95%	-	S211	81%	61%	F307	89%	90%
F307	52%	60%	V102	40%	-	N310	-	61%	S211	100%	93%
N310	53%	54%	F306	68%	72%	F306	85%	42%	S212	95%	-
			N310	94%	52%				N310	-	85%
			V326	54%	-				N329	83%	77%

[a]AC: Active, [b]IN: Inactive

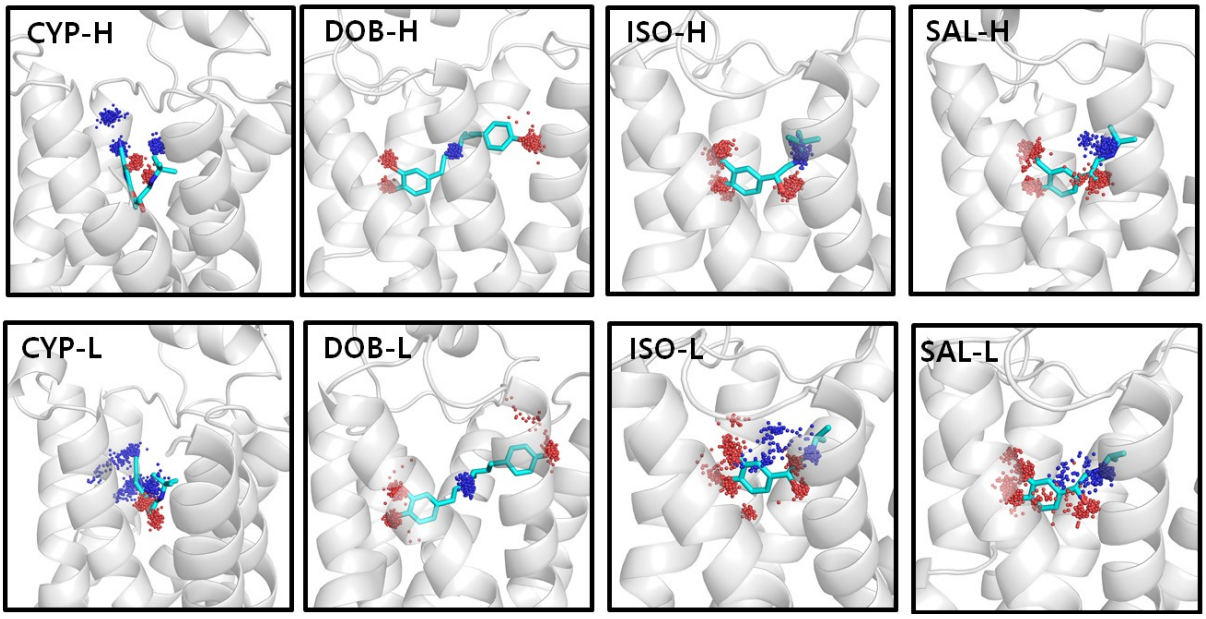

SI Figure S2. (Related to main Figure 2) Spatial distribution function (SDF) as the mobility estimation of selective agonists in the inactive and active states of β_1AR. SDF of the selected agonists calculated centering on the nitrogen atom (as a blue dot) and the oxygen atom (as a red dot) of each ligand.

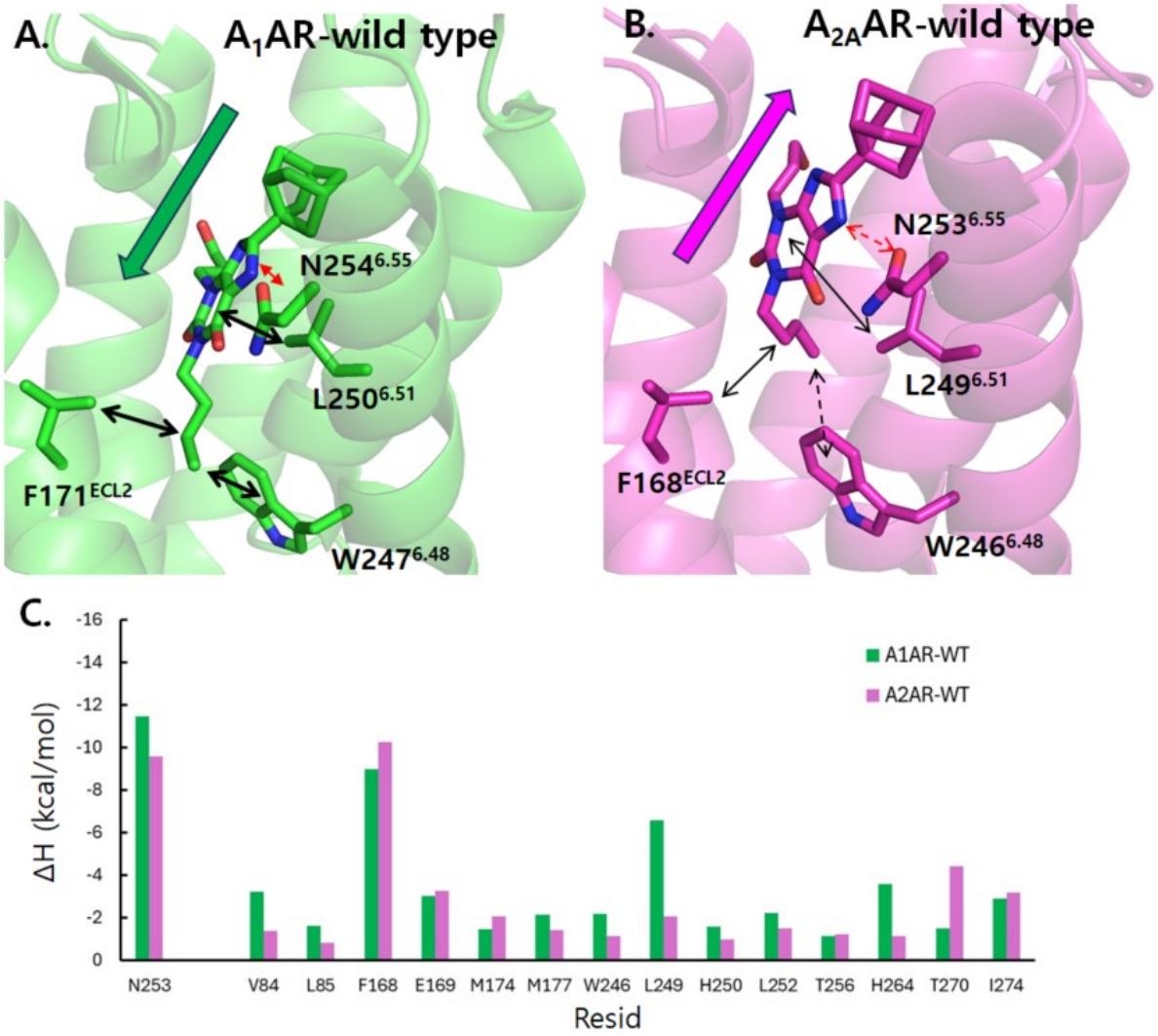

SI Figure S3. (related to main Figure 3). PSB36 ligand contacts with A_1AR-WT (**A**) and A_{2A}AR-WT (**B**), and non-bonded interaction energy between ligand and the residues in the binding site of A_1AR-WT (green) and A_{2A}AR-WT (magenta) (**C**).

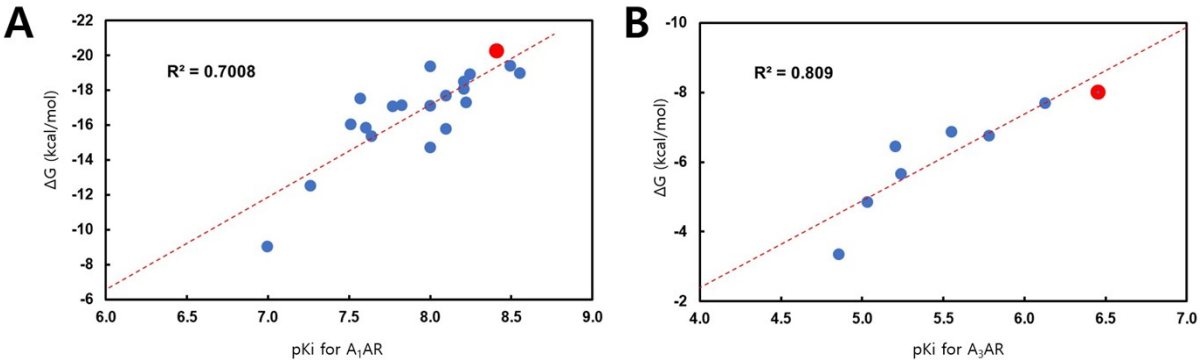

SI Figure S4. (Related to main Figure 5). Binding free energy calculations of antagonist derivatives bound to A_1AR and A_3AR. **A-B**. Correlation between the calculated binding free energies of A_1AR-derivatives (**A**) and A_3AR-derivatives (**B**) with their experimental K_i values. For Figure 5 in the main text, we re-scaled the X- and Y-axes uniformly to visualize the relative binding strengths of the derivatives for A_1AR and A_3AR more clearly.

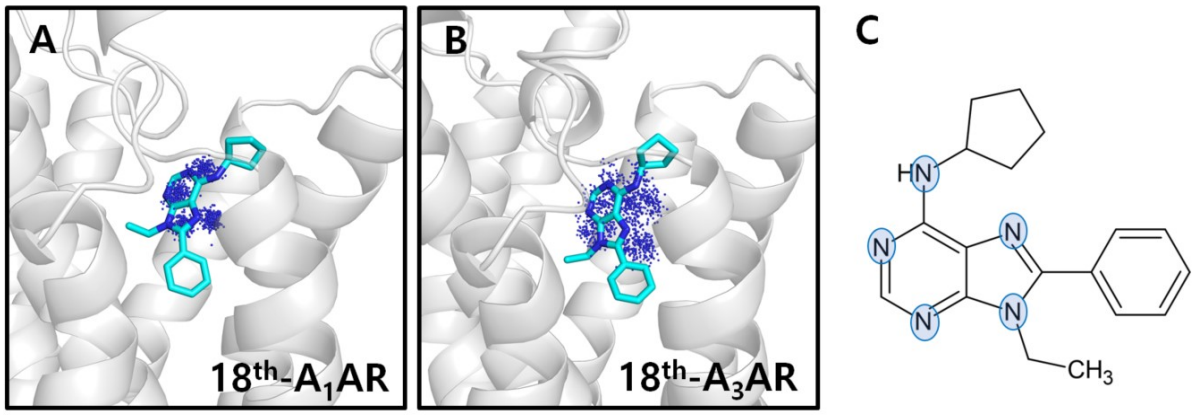

SI Figure S5. (Related to main Table 2 and main Figure 5). Analysis of Spatial distribution function (SDF) for 18th derivative bound to A_1AR and A_3AR complexes, respectively (**A-B**). SDF calculation was centered on the nitrogen atom from main scaffold, blue circles in **C**.

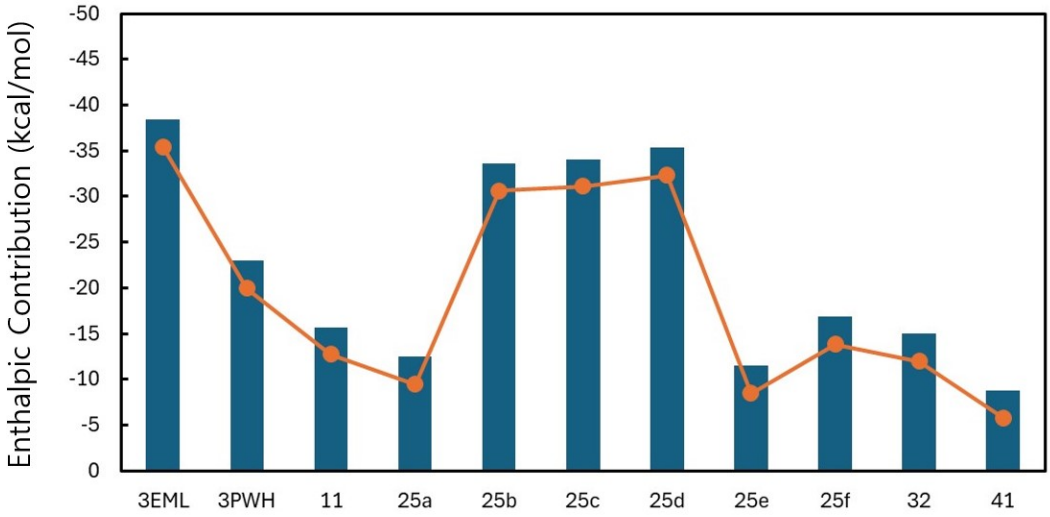

SI Figure S6. (Related to main Table 2 and main Figure 5). The enthalpic contribution (ΔH) expressed as the non-bonded interaction (the sum of electrostatic and van der Waals terms) using the entire MD trajectory of 11 systems for Case 4 study.

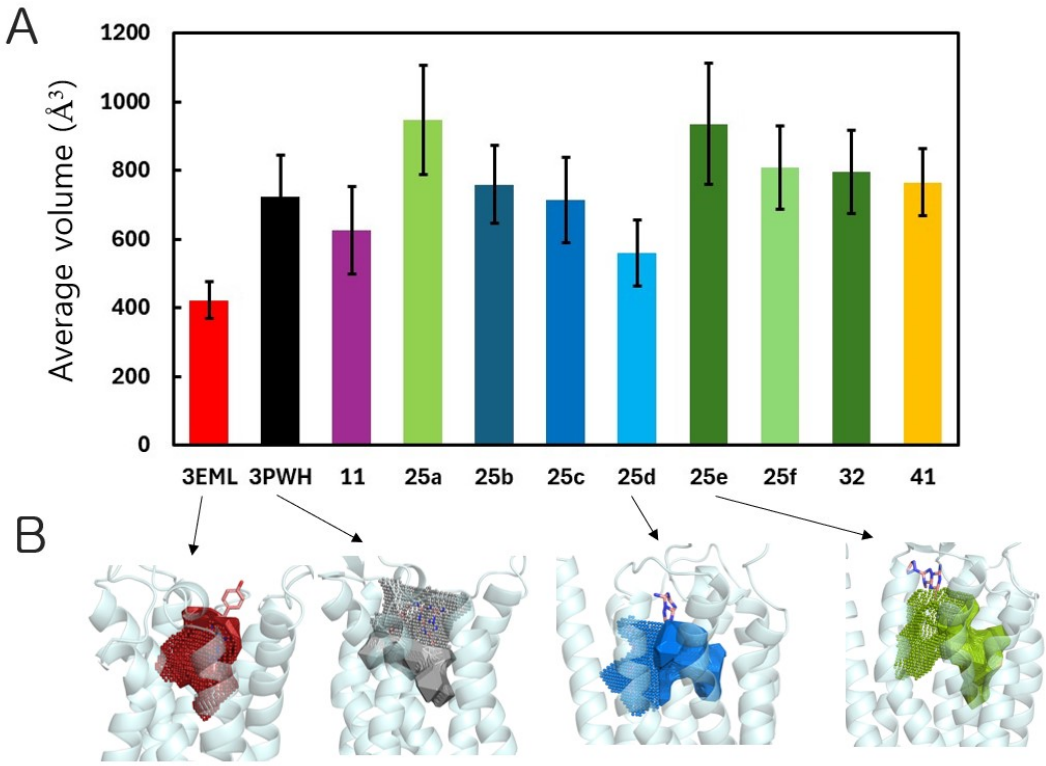

SI Figure S7. (Related to main Table 2 and main Figure 5). **A**. The average volume of the ligand binding site in a total of 11 A_{2A}AR systems studied for Case 4. All calculations were carried out by program POVME. **B**. The ligand volume representations with representative structures (extracted from the most populated cluster) of A_{2A}AR bound to ZMAs in the wild type (red), thermostabilized mutant (black), 25d (cyan), and 25e (dark green) derivatives.